

Warping and cracking of the Pacific plate by thermal contraction

David Sandwell and Yuri Fialko

Scripps Institution of Oceanography, University of California, San Diego, La Jolla, California, USA

Received 16 March 2004; revised 15 July 2004; accepted 2 August 2004; published 26 October 2004.

[1] Lineaments in the gravity field and associated chains of volcanic ridges are widespread on the Pacific plate but are not yet explained by plate tectonics. Recent studies have proposed that they are warps and cracks in the plate caused by uneven thermal contraction of the cooling lithosphere. We show that the large thermoelastic stress produced by top-down cooling is optimally released by lithospheric flexure between regularly spaced parallel cracks. Both the crack spacing and approximate gravity amplitude are predicted by elastic plate theory and variational principle. Cracks along the troughs of the gravity lineaments provide conduits for the generation of volcanic ridges in agreement with new observations from satellite-derived gravity. Our model suggests that gravity lineaments are a natural consequence of lithospheric cooling so that convective rolls or mantle plumes are not required. *INDEX TERMS*: 1208 Geodesy and Gravity: Crustal movements—intraplate (8110); 1236 Geodesy and Gravity: Rheology of the lithosphere and mantle (8160); 1219 Geodesy and Gravity: Local gravity anomalies and crustal structure; 3045 Marine Geology and Geophysics: Seafloor morphology and bottom photography; 8159 Tectonophysics: Rheology—crust and lithosphere; *KEYWORDS*: thermal contraction, Pacific plate, gravity anomalies

Citation: Sandwell, D., and Y. Fialko (2004), Warping and cracking of the Pacific plate by thermal contraction, *J. Geophys. Res.*, 109, B10411, doi:10.1029/2004JB003091.

1. Introduction

[2] Plate tectonics explains most of the topography of the deep ocean basins, but there is still debate regarding the origin of off-ridge features that are younger than the ambient lithosphere, and especially those that are not aligned with the autochthonic seafloor spreading fabric. The Pacific basin contains three main types of the young off-ridge lineaments (Figure 1). (1) Chains of shield volcanoes such as the Hawaiian-Emperor seamounts are well explained by the mantle plume model [Morgan, 1971; Sleep, 1992]. (2) Gravity lineaments are prominent at 140–200 km wavelength and are aligned in the direction of absolute plate motion [Haxby and Weissel, 1986] (Figure 1b). (3) En echelon volcanic ridges appear to be related to the gravity lineaments (Figure 2) and have morphology consistent with the ridge-parallel extensional stress [Lynch, 1999; Sandwell et al., 1995; Winterer and Sandwell, 1987] (Figure 3). The origin of both the gravity lineaments and the linear volcanic ridges has been the subject of many studies and field experiments [Dunbar and Sandwell, 1988; Fleitout et al., 1989; Forsyth et al., 2002; Gans et al., 2003; Haxby and Weissel, 1986].

[3] Several mechanisms have been proposed to explain the gravity lineaments (Figure 4), including small-scale convective rolls [Haxby and Weissel, 1986]; mini hot spots [Fleitout et al., 1989]; extension of the lithosphere or boudinage [Dunbar and Sandwell, 1988]; and thermal

bending stress caused by top-down cooling of the lithosphere [Gans et al., 2003]. Radiometric ages of the Puka-puka ridges in the central Pacific are inconsistent with the mini hot spot model [Sandwell et al., 1995]. The morphology of these volcanic ridges indicates that magma is extruded along cracks that are parallel to the absolute plate motion direction. Also, the chemistry of the dredged basalts is inconsistent with deep melting of plume material [Janney et al., 2000]. The small-scale convection model predicts extension and volcanism on the crests of the gravity lineaments but qualitative observations show that the volcanic ridges preferentially occur in the troughs [Forsyth et al., 2002; Sandwell et al., 1995; Searle et al., 1995; Winterer and Sandwell, 1987]. The boudinage model correctly predicts the characteristic wavelength of the gravity lineaments and the location of the volcanic ridges but at least 10% extension is needed to explain their observed amplitude [Dunbar and Sandwell, 1988]. Plate tectonic measurements of fracture zone spacing show that this amount of relative extension did not occur [Goodwillie and Parsons, 1992] and a recent study limits the extension to less than 2% [Gans et al., 2003]. Thus the alternative explanations are certainly warranted. Here we provide new observational evidence and theoretical arguments indicating that both the gravity lineaments and volcanic ridges result from cooling and thermal contraction of the oceanic lithosphere, and are a natural consequence of plate tectonics.

[4] Cooling and shrinkage of the oceanic lithosphere is a well-understood phenomenon that is responsible for the increase in seafloor depth with age [Parsons and Sclater, 1977]. Nonuniform shrinkage of the plate, mostly driven by

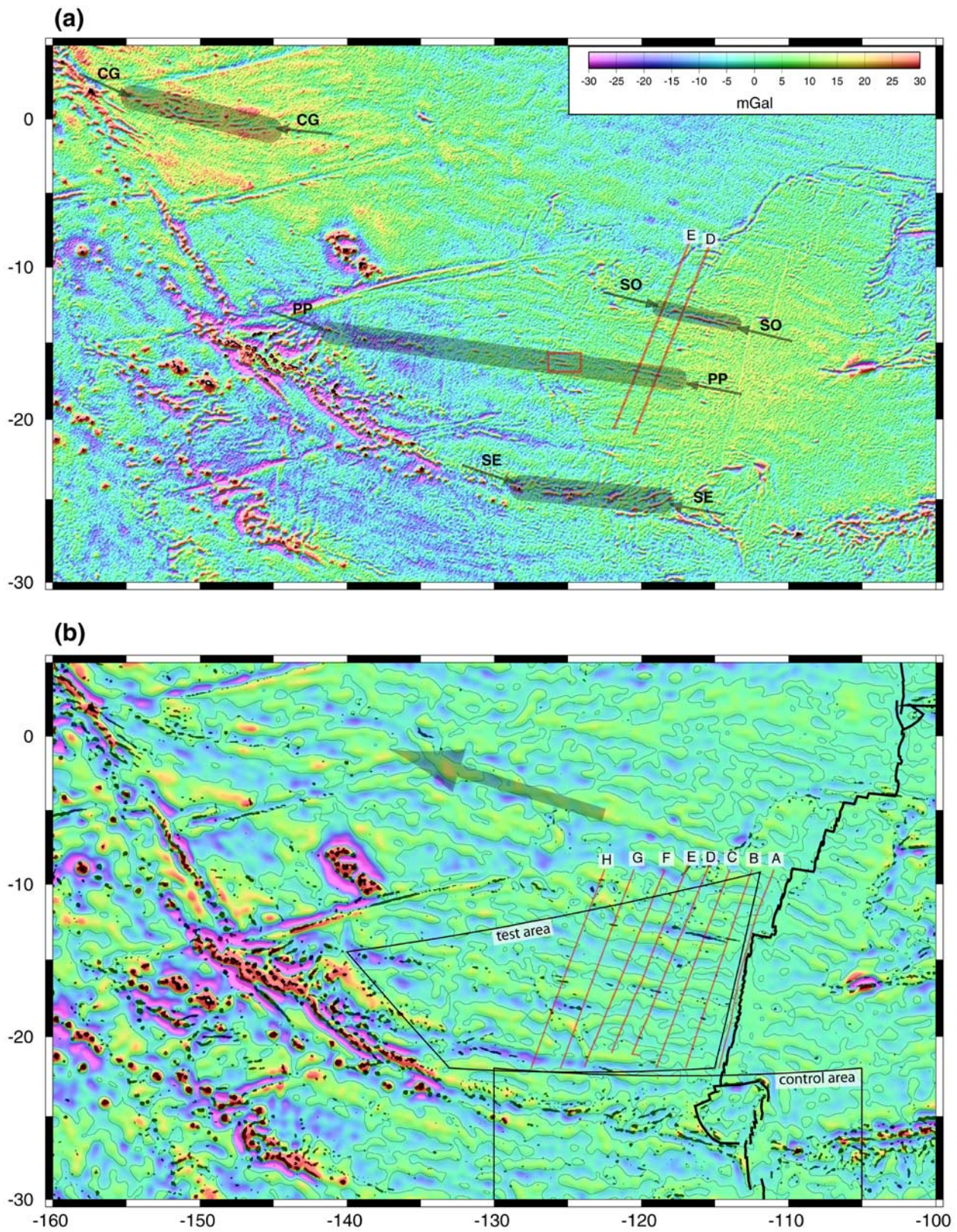


Figure 1

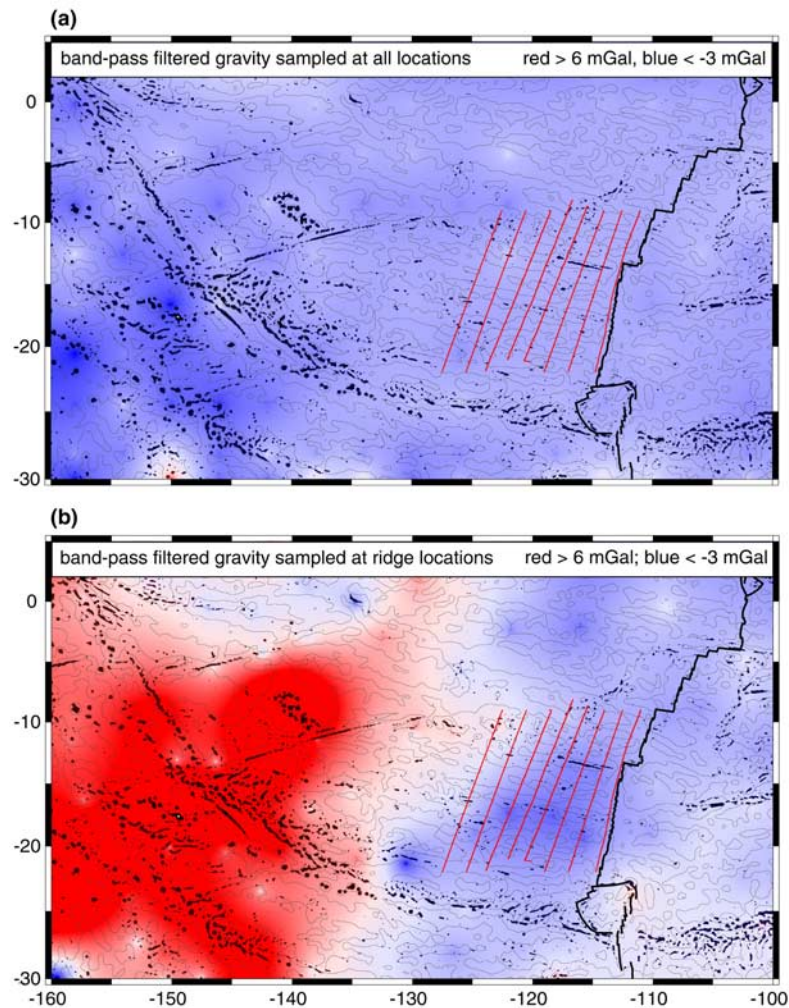


Figure 2. (a) Band-pass filtered gravity anomaly ($80 < \lambda < 600$ km) sampled at all locations and median filtered over a diameter of 450 km (red > 6 mGal; blue < -3 mGal). Because the band-pass filtered data are evenly sampled they have nearly zero mean and median everywhere. (b) Band-pass filtered gravity anomaly ($80 < \lambda < 600$ km) sampled at locations of volcanic ridges and seamounts and median filtered over a diameter of 450 km (red > 6 mGal; blue < -3 mGal). Airy and flexural compensation models predict the band-pass filtered gravity should be >1.5 mGal at volcanic loads. Areas of pronounced gravity lineaments have negative band-pass filtered gravity at volcanic ridges.

Figure 1. (a) Gravity anomaly derived from retracked ERS-1 radar altimeter data, Geosat altimeter data, and Topex altimeter data provides improved accuracy and resolution to reveal the close association between the gravity lineaments and the volcanic ridges. Red lines are track lines of R/V *Conrad* where bathymetry and gravity profiles were collected (see Figures 5 and 6). Red box outlines a part of the Pukapuka ridges that was surveyed by R/V *Melville* (see Figure 3) [Sandwell *et al.*, 1995]. Prominent volcanic ridges in the area include cross-grain ridges [Winterer and Sandwell, 1987] CG; Pukapuka ridges [Sandwell *et al.*, 1995] PP; the ridges of Searle *et al.* [1995] SE; and most recently the Sojourn Ridges [Forsyth *et al.*, 2002] SO. (b) Band-pass filtered gravity anomaly ($80 < \lambda < 600$ km) derived from retracked satellite altimeter data. Color scale saturates at ± 15 mGal. Gravity lineaments with 140-km wavelength develop between the ridge axis and 6 Ma (Profile C) and are oriented in the direction of absolute plate motion (large arrow). Lineaments on older seafloor have somewhat longer wavelength (~ 180 km) and cross the grain of the seafloor spreading fabric. Gravity lineaments also occur on the Nazca plate to the east of the East Pacific Rise. Seamounts and volcanic ridges are marked as black areas. Many of these volcanic chains are geometrically associated with the gravity lineaments. The morphology of three sets of these ridges indicates that they formed by N-S tension of the Pacific plate [Lynch, 1999]. The longest of these ridge groups, the Pukapuka ridges, extends for over 2600 km from 5 Ma old seafloor near the East Pacific Rise to 45 Ma old seafloor near the Tuamotu Archipelago.

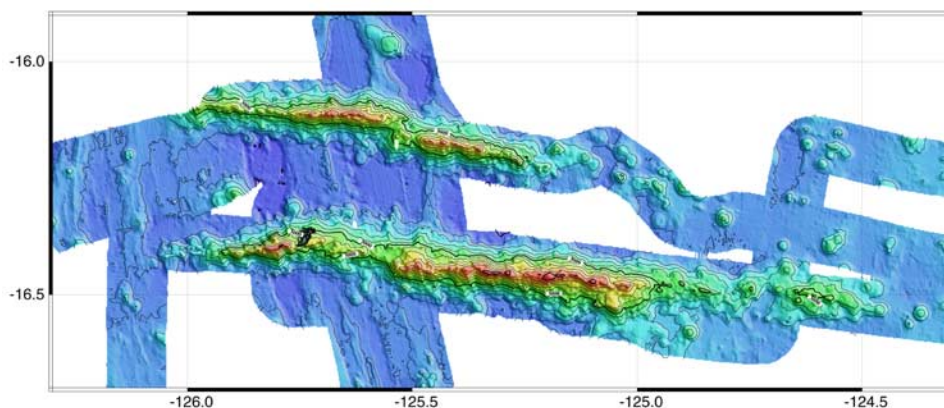


Figure 3. Detailed bathymetry (200-m contour interval) of a pair of volcanic ridges along the Pukapuka chain [Sandwell *et al.*, 1995]. The ridges are about 2 km tall, 10 km wide and 75/150 km long. These ridges formed 9 Ma ago and are on seafloor that is 19 Ma. Notice that the ridges are not perpendicular to the abyssal hill fabric.

the temperature gradients in the top part of the lithosphere, results in the development of thermoelastic stresses that are large enough to fracture the plate [Bratt *et al.*, 1985; Parmentier and Haxby, 1986; Sandwell, 1986; Turcotte, 1974; Wessel, 1992]. Because the thickness of the lithosphere is small compared to its horizontal dimensions, and the seafloor is a stress-free boundary, the vertical component of the deviatoric stress is small and can be neglected. Under the thin plate approximation, the horizontal components of thermoelastic stress can be decomposed into a thermal end load and a thermal bending moment [Boley and Weiner, 1960]. The thermal end loads can be partially relieved by plate-wide shrinkage, especially near the ridge axis, which is unable to support large deviatoric stresses [Fialko, 2001; Parsons and Thompson, 1991]. However, even a plate with free ends may experience large thermoelastic stress, with compressional stress near the surface and tensional stress at depth [Parmentier and Haxby, 1986; Wessel, 1992]. The same physics describes tempering of glass sheets, whereby the residual compression at the surface inhibits the development of tensile fractures [Woo, 1968]. The predicted pattern of thermoelastic deformation is consistent with the focal mechanisms of intraplate earthquakes [Bergman and Solomon, 1984; Shen *et al.*, 1997; Wiens and Stein, 1984]. Recently, Gans *et al.* [2003] proposed that the gravity lineaments are caused by convex upward flexure of the plate between regularly spaced lithospheric cracks where the flexure is driven by thermoelastic bending moments. While their model shows fair agreement with the observations, it does not explain why cracks develop with a particular spacing; Gans *et al.* [2003] assume a 150-km spacing to match the observed spacing.

[5] Here we test and refine the thermal contraction model to explain the origin of both the volcanic ridges and the gravity lineaments through a quantitative analysis of gravity data, as well as by developing a numerical model of thermoelastic flexure. We address the following questions. (1) How do the gravity lineaments develop in amplitude and wavelength as a function of seafloor age? (2) Does the intraplate volcanism indeed preferentially occur in the troughs of the gravity lineaments? These first two questions

are addressed using the gravity anomalies derived from reprocessing of the raw radar waveforms of ERS-1 satellite altimeter data. (3) Is there sufficient thermal bending moment to explain the amplitudes of both the gravity

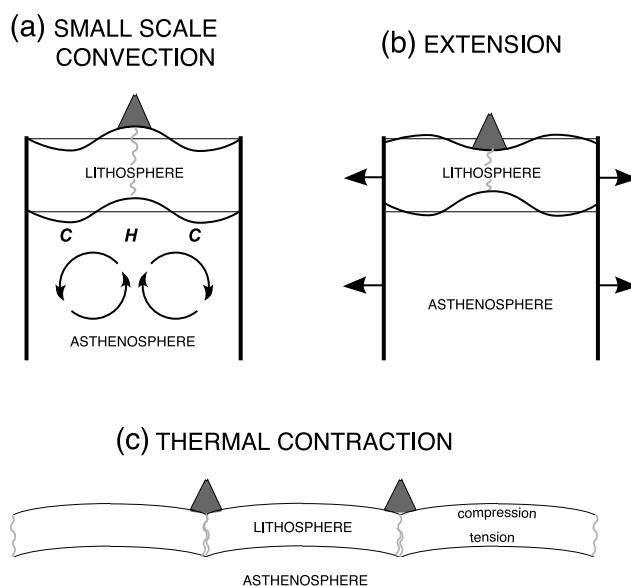


Figure 4. Models for the formation of the gravity lineaments and en echelon volcanic ridges. (a) Small-scale convection cells develop beneath cooled lithosphere and align in the direction of absolute plate motion by shear in the asthenosphere [Buck and Parmentier, 1986; Richter and Parsons, 1975]. Volcanoes develop above the hot upwelling axis of the cell. (b) Slow and diffuse extension creates lithospheric boudinage structures [Ricard and Froidevaux, 1986]. Volcanoes develop in the troughs (maximum strain) if partially melted mantle is available beneath the plate [Sandwell *et al.*, 1995]. (c) Thermoelastic flexure will develop if the lithosphere is cracked at a regular intervals [Gans *et al.*, 2003]. Volcanoes will develop above the cracks if partially melted mantle is available beneath the plate.

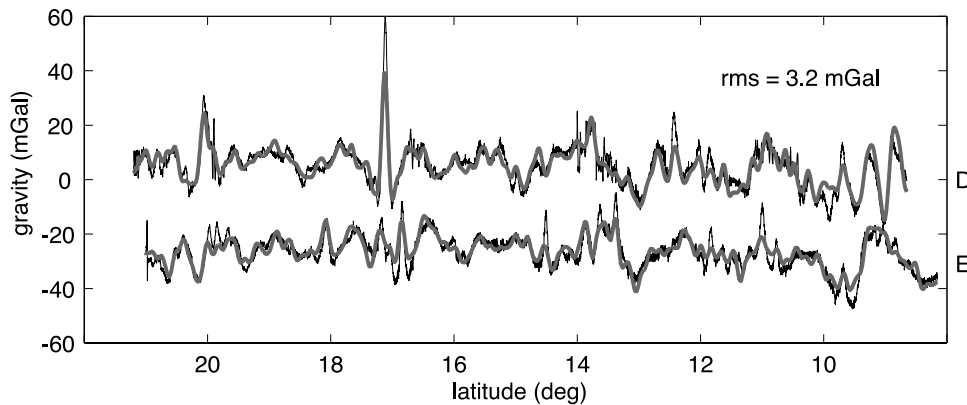


Figure 5. Comparison between shipboard (black) and satellite-derived (gray) gravity anomalies along profiles D and E (Figure 1) [Abers *et al.*, 1988] has 3.2 mGal RMS deviation. The improved resolution and accuracy of the retracked ERS-1 altimeter data is used to better delineate the volcanic ridges.

lineaments and the associated topography? (4) Finally, what mechanism controls the regular spacing of cracks of the order of the flexural wavelength? One of the most important aspects of the thermoelastic model is that both the amplitude and spacing of the gravity lineaments are predicted from quantifying a process that is fundamental to plate tectonics, namely, the thermal contraction of the oceanic lithosphere.

2. Gravity Lineaments and Volcanic Ridges From Satellite Altimetry

[6] The central Pacific gravity lineaments were first discovered from the analysis of Seasat altimeter data [Haxby and Weissel, 1986]. While the track spacing and resolution of the Seasat data was sufficient to reveal the 140–200 km gravity lineaments, the discovery of volcanic ridges required better coverage and higher precision. The ERS-1 satellite altimeter increased the coverage during its geodetic phase (1994–95) and the higher quality Geosat altimeter data were declassified in 1995 [Sandwell and Smith, 1997]. Since the volcanic ridges are typically only 20 km wide and usually less than 1000 m tall, most were not visible above the 5–7 mGal noise level in the altimeter-derived gravity anomaly maps. Guided by these noisy gravity maps, several sets of ridges were surveyed by multibeam sonar (Figure 1a, shaded areas): cross-grain ridges [Winterer and Sandwell, 1987]; Pukapuka ridges [Sandwell *et al.*, 1995]; the ridges of Searle *et al.* [1995]; and most recently the Sojourn Ridges [Forsyth *et al.*, 2002]. These sets of ridges appear to be preferentially located in the troughs of the gravity lineaments although there has been no quantitative confirmation of this observation.

[7] To confirm the spatial correlation between the ridges and the gravity lineaments, we improve the resolution of the ERS-1 altimeter data by retracking the raw altimeter waveforms [Maus *et al.*, 1998] (Figure 1a). The retracking increases the short-wavelength precision by nearly a factor of 2, so the quality of the ERS-1 data is now superior to the Geosat data (not retracked yet). A new gravity model was constructed using all available altimeter profiles (see version 11 at <http://topex.ucsd.edu>). The RMS deviation between two shipboard profiles and the new gravity model is 3.2 mGal in this area (Figure 5).

[8] The gravity field of the small-scale ridges was separated from the larger scale gravity lineaments using isotropic the filters in Generic Mapping Tools [Wessel and Smith, 1991] (Figure 1b). A two-step, low-pass filter was used to remove features with wavelength shorter than about 80 km. First a median filter was applied to remove the sharp gravity highs associated with seamounts and ridges. This filter replaced each gravity value with the median of all of the values in a 65-km diameter circle. The second filter (applied in the wave number domain) passed wavelengths greater than 108 km and cut wavelengths less than 54 km using a cosine taper to attain a 0.5 gain at 80 km. The high-pass filtered gravity (total minus low-pass gravity) was clipped at 10 mGal to identify volcanic features (black areas in Figures 1b and 2). The clipping amplitude was selected to best match the outline of the volcanic edifices that have been mapped during multibeam bathymetry surveys [Forsyth *et al.*, 2002; Lynch, 1999] without introducing spurious features. To further isolate the gravity lineaments, the low-pass filtered part of the gravity field was high-pass filtered for wavelengths greater than 600 km (cosine taper 1200–600 km). Note that the passband of the filter (108–600 km) was selected to be outside the wavelength band of the gravity lineaments 120–300 km. Also note that while isotropic filters were used, the residual fields are highly anisotropic; both the gravity lineaments and ridges are oriented in approximately the direction of the absolute motion of the Pacific plate over the Hawaiian hot spot (Figure 1b).

[9] Profiles of band-pass filtered gravity reveal the development of the gravity lineaments on young seafloor (Figure 6). The profile closest to the East Pacific Rise (EPR) has very low amplitude and little, if any, periodic variations in the gravity field. The next profile to the west (3.2 Ma) reveals partially developed gravity lineaments (5 mGal peak-to-trough amplitude and 120 km wavelength). The amplitude and wavelength of the gravity lineaments increases with increasing seafloor age; by 8.2 Ma they are fully developed (10 mGal amplitude and 160-km wavelength). There is an indication that the wavelength increases to about 200 km on older seafloor. The gravity lineaments cut across the grain of the older seafloor (>20 Ma) indicating they are younger than the ambient lithosphere.

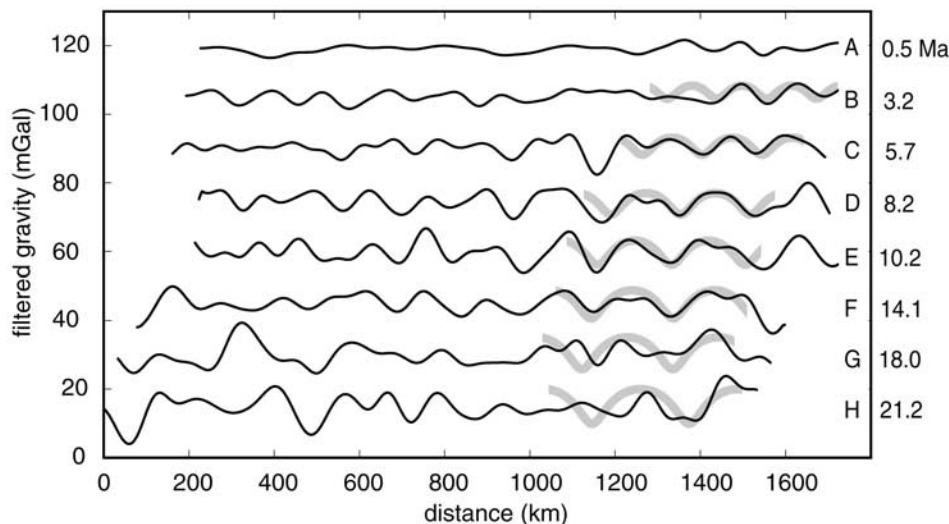


Figure 6. Satellite-derived gravity profiles parallel to the East Pacific Rise crest reveal the development of the gravity lineaments. Two-dimensional filtering of the satellite-derived gravity reveals the development of the seafloor undulations. Undulations are not apparent at the ridge axis (profile A) but develop rapidly on 3.2 Ma seafloor (Profile B) and are fully developed on 7–12 Ma seafloor. Model predictions (gray lines) match the wavelength of the observed seafloor undulations between 0 and 12 Ma. A good amplitude match is obtained by reducing the model amplitude by a factor of 0.75. On older seafloor (>14 Ma), the model overpredicts both the amplitude and wavelength of gravity lineaments.

[10] A visual examination of the area of most intense gravity lineaments suggests that the volcanic ridges are preferentially located in the troughs (Figure 1b, test area). Here we provide a quantitative confirmation of this observation. However, before investigating this relationship between volcanic ridges and gravity lineaments, it is instructive to consider the expected gravity field of a ridge in the absence of gravity lineaments. All models for the gravity field above seafloor topography (e.g., Airy, Pratt, flexural, and thermal isostasy models) have a positive gravity-to-topography ratio at all wavelengths. Therefore no matter how the data are band-pass filtered, the gravity anomaly should always be positive above the crest of a volcanic ridge. To further confirm and quantify this statement, we performed a simulation of flexural loading of a 5-km thick elastic plate [Goodwillie and Watts, 1993] using our identified distribution of volcanic ridges in the test area. The height of each volcano was derived from the predicted bathymetry map [Smith and Sandwell, 1997]. In the absence of gravity lineaments, the model predicts a 1.57 mGal shift in the ridge-sampled, band-pass filtered gravity.

[11] We use two approaches to show that the volcanic ridges in the area of most intense gravity lineaments (test area in Figure 1) are not randomly dispersed with respect to the gravity lineaments. First we sample the band-pass filtered gravity at every location and median-filter the data over a 450-km diameter area. As expected the mean and median of the band-pass filtered gravity is close to zero everywhere (Figure 2a). However, if we sample only at the locations of the volcanic features, distinct patterns emerge (Figure 2b). Areas of large volcanoes and islands, west of -135° longitude, are preferentially associated with positive,

band-pass filtered gravity anomalies as expected. Smaller volcanoes (~ 1000 m tall), east of 135° longitude, are preferentially associated with moderately positive, band-pass filtered gravity except in the areas of intense gravity lineaments where they preferentially associated with valleys of the gravity lineaments (blue are in Figure 2b).

[12] To further quantify this analysis, we examine the statistics of these samples by selecting three areas (Figure 7). The test area was selected to contain the most prominent gravity lineaments. The control area was selected to be on similar age seafloor as the test area and have numerous small volcanic features. We also provide statistics for the entire area. First we make histograms of the area covered by volcanic ridges as a function of the band-pass filtered gravity and compute the mean and standard deviation of the histograms (Figure 7). For the entire area, the mean is 6.85 mGal and the standard deviation is 16.18 mGal. The positive mean confirms the discussion above that band-pass filtered gravity is expected to be positive above volcanic ridges. The large standard deviation is also expected because of the wide range of volcano sizes that populate the entire area. Volcanic ridges in the control area have a positive mean value of 1.39 mGal in agreement with the flexure model simulation above and a standard deviation of 4.10 mGal reflecting a smaller range of volcano sizes. Volcanic ridges in the test area have mean of -0.98 mGal and a standard deviation of 3.88 mGal. The negative mean value is unexpected and in discordance with the compensation models discussed above. Could the difference in mean value, between the test area and the control area (-2.37 mGal), be a statistical fluke? To calculate the probability of this occurring by chance, one needs to

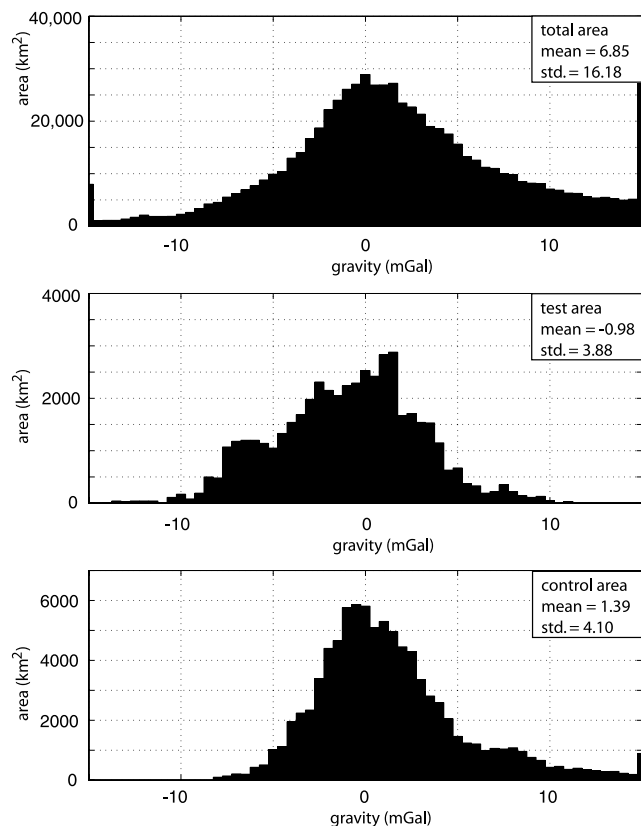


Figure 7. Histograms of the area of volcanic ridge seafloor versus band-pass filtered gravity. (top) The histogram of the part of the total area that is covered by volcanoes has a mean of 6.85 and a standard deviation of 16.18. (middle) The histogram of the test area covered by prominent volcanoes (see Figure 1) has a mean of -0.98 and a standard deviation of 3.88. (bottom) The histogram of the portion of the control area covered by prominent volcanoes has a mean of 1.39 and a standard deviation of 4.10. This difference in mean gravity between the test area and the control area (-2.38 mGal) is consistent with the hypothesis that volcanic ridges in the test area preferentially occur in the troughs of the gravity anomalies.

calculate the uncertainty in the mean of the test area, which is equal to the standard deviation divided by the square root of the number of independent samples (volcanoes). We count 224 independent volcanoes (30-km diameter circle) in the test area so uncertainty in the mean is 0.26 mGal. Therefore the difference of the means of the two populations is 9 times the uncertainty in the mean clearly ruling out a random coincidence. Even if we overestimated the volcano count by a factor of 10 (so there are only 22 independent volcanoes) then the mean difference is still 2.9 times the uncertainty in the mean resulting in a probability of 1 in 535 of this occurring by chance. This demonstrates that the volcanic ridges are indeed preferentially located in the troughs of the gravity lineaments.

[13] On the basis of this analysis, one could propose that volcanic ridges occur in the troughs because they preferentially create or intensify the gravity lineaments. There are two arguments against this proposition. First the

troughs of most gravity lineaments do not contain volcanic ridges. Second, as shown by *Goodwillie and Watts* [1993], the flexural response from even the largest volcanic loads are insufficient to create the gravity signatures of the gravity lineaments. We are left with the hypothesis that gravity lineaments reflect the primary physical process and the volcanic ridges are a possible consequence of this process. Moreover, this process preferentially produces volcanic ridges in the troughs of the gravity lineaments. We believe these observations rule out a small-scale convective origin for the gravity lineaments and ridges.

3. Thermoelastic Cracking of the Lithosphere

[14] *Turcotte* [1974] proposed that thermal stresses caused by cooling of the lithosphere may be responsible for transform faults which act to relieve the stress. He provided an analytic solution for the plate flexure that will develop when the plate is subjected to bending moments at its edges. More recent studies [*Parmentier and Haxby*, 1986; *Wessel*, 1992] have noted that if the plate is free to contract while it is cooling, a downward bending moment will increase almost linearly with the age of the plate. The upper third of the plate will be in compression while the lower two thirds will be in tension. These calculations consider the finite yield strength of the lithosphere which becomes especially important in limiting the near surface stress. *Gans et al.* [2003] use these estimates of increasing thermal bending moment and *Turcotte's* analytic flexure solution to explain the amplitude of the gravity lineaments in the Pacific plate. For a crack spacing of 150 km their calculations shows the development of 100 m of peak-to-trough plate flexure at an age of 3 Ma. However, their model does not explain the observed crack spacing and it also underestimates the amplitudes of the gravity lineaments. Here we present a theoretical model of yielding of the thermoelastically deformed lithosphere that is based on the variational principle. In particular, we postulate that the lithosphere will deform in a way that will minimize the overall mechanical energy stored in a plate. We search for the crack spacing that liberates the maximum mechanical energy, and show that the optimal crack spacing is of the order of the flexural wavelength.

[15] Consider a plate of length L with ends subjected to a bending moment M_T due to accumulation of thermoelastic stress. *Turcotte* [1974] provides an analytic solution for the deflection of a thin elastic plate floating on a fluid half space of density ρ (3300 kg m^{-3}). The plate deflection w , and curvature w'' , are

$$\begin{aligned} w(x) &= A \cos \frac{x}{\alpha} \cosh \frac{x}{\alpha} + B \sin \frac{x}{\alpha} \sinh \frac{x}{\alpha} \\ w''(x) &= \frac{-2A}{\alpha^2} \sin \frac{x}{\alpha} \sinh \frac{x}{\alpha} + \frac{2B}{\alpha^2} \cos \frac{x}{\alpha} \cosh \frac{x}{\alpha} \end{aligned} \quad (1)$$

where $\alpha = \left(\frac{4D}{\Delta\rho g}\right)^{1/4}$ is the flexural parameter, $D = \frac{EH^3}{12(1-\nu^2)}$ is the flexural rigidity, E is the Young's modulus (65 GPa), H is the plate thickness, ν is the Poisson's ratio (0.25), $\Delta\rho$ is the density difference between mantle and seawater, and g is

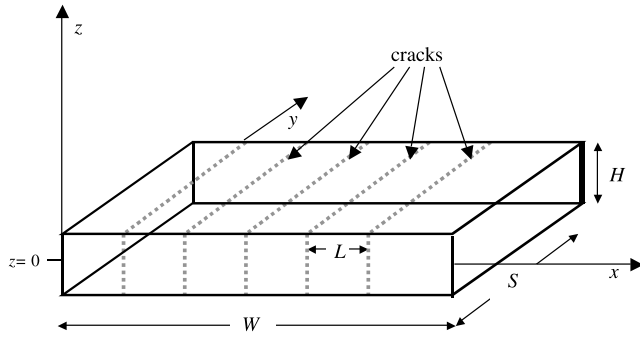


Figure 8. Thin elastic plate of thickness H , length S , and width W , contains N cracks with spacing of L .

the acceleration of gravity (9.8 m s^{-2}). The coefficients A and B are given by

$$A = \frac{\cos \theta \sinh \theta - \sin \theta \cosh \theta M_T \alpha^2}{\sin \theta \cos \theta + \sinh \theta \cosh \theta 2D} \quad (2)$$

$$B = \frac{\cos \theta \sinh \theta + \sin \theta \cosh \theta M_T \alpha^2}{\sin \theta \cos \theta + \sinh \theta \cosh \theta 2D}$$

where $\theta = \frac{L}{2\alpha}$.

4. Energy Released by Flexure

[16] To predict the optimal crack spacing we calculate the energy released by the flexure. The change in the potential energy of elastic deformation stored in a plate is $F = \int_V \sigma(\mathbf{x})\varepsilon(\mathbf{x})dV$, where σ is the stress perturbation, and ε is the strain perturbation about some reference (e.g., lithostatic) state of deformation, and the integration is performed over the entire plate volume V [Boley and Weiner, 1960, p. 262]. Prior to the onset of flexure, the stress σ equals the thermoelastic stress $\sigma_T(z)$ induced by the plate cooling, and the strain ε is zero. After cracking, individual segments of the plate will experience elastic flexure such that the change in stress and strain components may be written as

$$\begin{array}{ll} \text{initial} & \text{final} \\ \varepsilon(z) = 0 & \varepsilon(z) \end{array} \quad (3)$$

$$\sigma(z) = \sigma_T(z) \quad \sigma(z) = \sigma_T(z) + \frac{E}{(1-\nu^2)}\varepsilon(z)$$

For a quasistatic deformation, the change in energy Δf from the initial state to the final state is independent of path and equals

$$\Delta f = \frac{E(\Delta\varepsilon)^2}{(1-\nu^2)} + \sigma_T \Delta\varepsilon \quad (4)$$

The first term in equation (4) is the energy needed (consumed) to flex the plate while the second term is the thermoelastic energy released. Now consider the net energy released when equally spaced cracks are introduced in a cooled plate subject to thermoelastic prestress σ_T (Figure 8).

The plate has length S and width W and contains N longitudinal cracks with spacing L . The total elastic energy released, normalized by the area of the plate, is the energy density Q and it is given by

$$Q = \frac{F}{SW} = \frac{1}{SW} \iiint_V \sigma(\mathbf{x})\varepsilon(\mathbf{x})dzdxdy \quad (5)$$

Noting that the problem is plane strain (there is no deformation along the y axis), and $L = W/N$, one can rewrite the energy density as

$$Q = \frac{1}{L} \int_{-L/2}^{L/2} \int_{-H/2}^{H/2} \sigma(x,z)\varepsilon(x,z)dzdx \quad (6)$$

We expand the integrand in equation (6) using the expressions for energy change (4). For a thin plate flexure, $\varepsilon(z) = -zw''$, where z is the distance from the center of the plate and w'' is the plate curvature given in equation (1). The integral (6) becomes

$$Q = \frac{1}{L} \left\{ \int_{-L/2}^{L/2} [w''(x)]^2 \int_{-H/2}^{H/2} \frac{E}{(1-\nu^2)} z^2 dz dx - \int_{-L/2}^{L/2} w''(x) \cdot \int_{-H/2}^{H/2} \sigma_T(z) z dz dx \right\} \quad (7)$$

The first term on the right-hand side of equation (7) is the energy consumed by flexure of the plate. The second term is the thermoelastic energy released during the flexure. Note that the integral over z in the first term is the flexural rigidity D while the integral over z in the second term is the thermal bending moment M_T . Thus expression (7) can be written as

$$Q = \frac{D}{L} \int_{-L/2}^{L/2} [w''(x)]^2 dx - \frac{M_T}{L} \int_{-L/2}^{L/2} w''(x) dx \quad (8)$$

For both terms, the energy depends on the curvature of the plate, but note that the energy consumed by plate flexure is always positive since it depends on the curvature squared while the thermoelastic energy released by flexure depends on the sign of the curvature. Concave downward flexure releases thermoelastic energy. By differentiating the expression (7) with respect to the crack spacing L , we find that Q has a global minimum at $L_c \approx 3.389\alpha$ (Figure 9), corresponding to the maximum energy release.

[17] It is reasonable to assume that in the presence of random variations in the lithospheric strength and initial yielding induced by thermoelastic stresses, the subsequent deformation will be eventually localized on the optimally spaced macroscopic fracture zones. The occurrence of volcanic ridges along the presumed translithospheric cracks suggests that the crack formation is caused (or assisted by) the magma fracture, whereby the ascending dikes relieve the deviatoric stress in the lithosphere. This mechanism implies

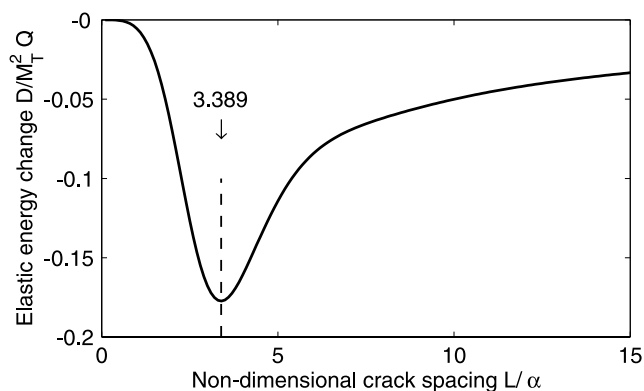


Figure 9. Model prediction for the thermoelastic energy release as a function nondimensional crack spacing L/α . Minimum in the potential energy of elastic deformation of the plate occurs when $L \approx 3.389 \alpha$.

that the crack zone is “weak” only during the dike emplacement; after the stress is reset and the magmatic activity ceases, the mechanical properties of a “cracked” plate do not differ substantially from those of an “intact” plate. Alternatively, the thermoelastic stresses might be relieved primarily by thrust and normal faulting in the shallow and deep sections of the plate, respectively. Even in this case the subsequent magma intrusions are likely to substantially reduce the deviatoric stresses in the lithosphere along the crack zones, as dikes won’t be able to deliver magma to the surface due to the negative dike buoyancy under the normal faulting conditions, and the unfavorable magma fracture orientation under the thrust faulting conditions. The dike intrusions will first relax the extensional stresses at the bottom of the plate, transferring the extension to shallower levels, and allowing the subvertical magma transport in the upper section of the plate. Regardless of whether the lithospheric crack zones are “hot” (magma induced) or “cool” (amagmatic), the crack spacing predicted by our model is controlled only by the flexural wavelength of the lithosphere, and is in excellent agreement with observations (Figure 6). Note that the volcanic activity associated with the inferred crack zones implies the presence of partial melt in the sublithospheric mantle. This melt may represent remnant magma not extracted from the mantle at the ridge axis, or reheating of the asthenosphere by plumes of the Superswell area [Janney *et al.*, 2000]. The orientation of cracks induced by the thermoelastic deformation is controlled by intraplate stresses. In particular, the cracks are predicted to align perpendicular to the least compressive stress.

5. Amplitude and Wavelength of Gravity Lineaments

[18] We use the method of Wessel [1992] to incrementally compute the evolution of thermoelastic stress as a function of depth. At each time step we allow the end load to relax to zero and then check that the stress does not exceed the yield strength envelope for dry olivine and pore water content of 0.5 [Goetze and Evans, 1979]. Our estimates of thermo-

elastic bending moment are 1.6 times greater than the estimates given by Gans *et al.* [2003] but are in agreement with Wessel’s calculations. The difference in the amplitudes is related to the assumption about the strength of the lower part of the thickening lithosphere. Gans *et al.* [2003] assume a sharp cutoff in strength at a temperature of 600°C, while Wessel [1992] used the full ductile flow law to define the strength. This difference results in small variations in strength at the base of the thickening plate which are amplified by the long moment arm to produce a 1.6 increase in thermoelastic moment.

[19] The results of our calculations are shown in Figure 10 where we allow thermoelastic bending moment M_T to develop for some period of time before the cracks with spacing L are introduced (the onset time). The flexural rigidity D at the onset time is computed using the portion of the plate where the yield strength exceeds 20 MPa which roughly corresponds to the depth to the 600°C isotherm. The corresponding values of D and M_T are then used in equation (1) to calculate the flexural topography. For this case of 130-km crack spacing, and 6 Ma onset time the peak-to-trough flexural amplitude is about 200 m and the filtered gravity amplitude is 5 mGal (Figure 10a). We also calculate the flexural energy consumed and the thermoelastic energy released as a function of distance perpendicular to the cracks for an onset time of 6 Ma (Figure 10b). The net energy released is zero near the ends of the flexure. This illustrates why the model discourages the small crack spacing as being unable to efficiently relieve the thermoelastic stress (although the thin plate approximation obviously becomes inapplicable when the crack spacing L is not large compared to the plate thickness H). Toward the center of the flexure the thermoelastic energy released is greater than the flexural energy consumed because the thermal prestress exceeds the flexural stress. Note that if the curvature of the plate becomes concave upward, the stress must increase in magnitude resulting in energy consumption. Therefore there is also an energy penalty when the crack spacing exceeds the critical wavelength L_c .

[20] Because the flexural parameter scales with the plate thickness, $\alpha \propto H^{3/4}$, the optimal crack spacing increases with the increasing age of the lithosphere (Figure 10c). So far we have assumed that the fracture energy required for the crack formation is negligible compared to the energy balance (8). Our dimensional estimates of the thermoelastic energy release seem to justify this assumption (Figure 10c). Although the in situ fracture energy E_F is not well known, and may be scale-dependent, we use values derived from the laboratory measurements (10^2 – 10^3 Jm $^{-2}$ for the tensile fracture energy [Atkinson, 1987; Fialko and Rubin, 1997]) and earthquake data (10^4 – 10^7 Jm $^{-2}$ for the shear fracture energy [Husseini, 1977; Scholz, 2002]) to place an upper bound on work spent on inelastic deformation. For the model shown in Figure 4c, the work spent on creating the cracks per unit area of the seafloor is $E_F H/L$. Thus the fracture energy enhances a penalty for the small crack spacing. Assuming $E_F = 10^7$ Jm $^{-2}$, $H = 15$ km, and $L = 150$ km, we obtain $E_F H/L \sim O(10^6)$ Jm $^{-2}$, i.e., small compared to the thermoelastic energy density Q for the lithosphere older than 1–2 Ma (10^7 – 10^8 Jm $^{-2}$, Figure 10c). However, the fracture energy might not be negligible in the lithosphere younger than 1 Ma. If the apparent absence of

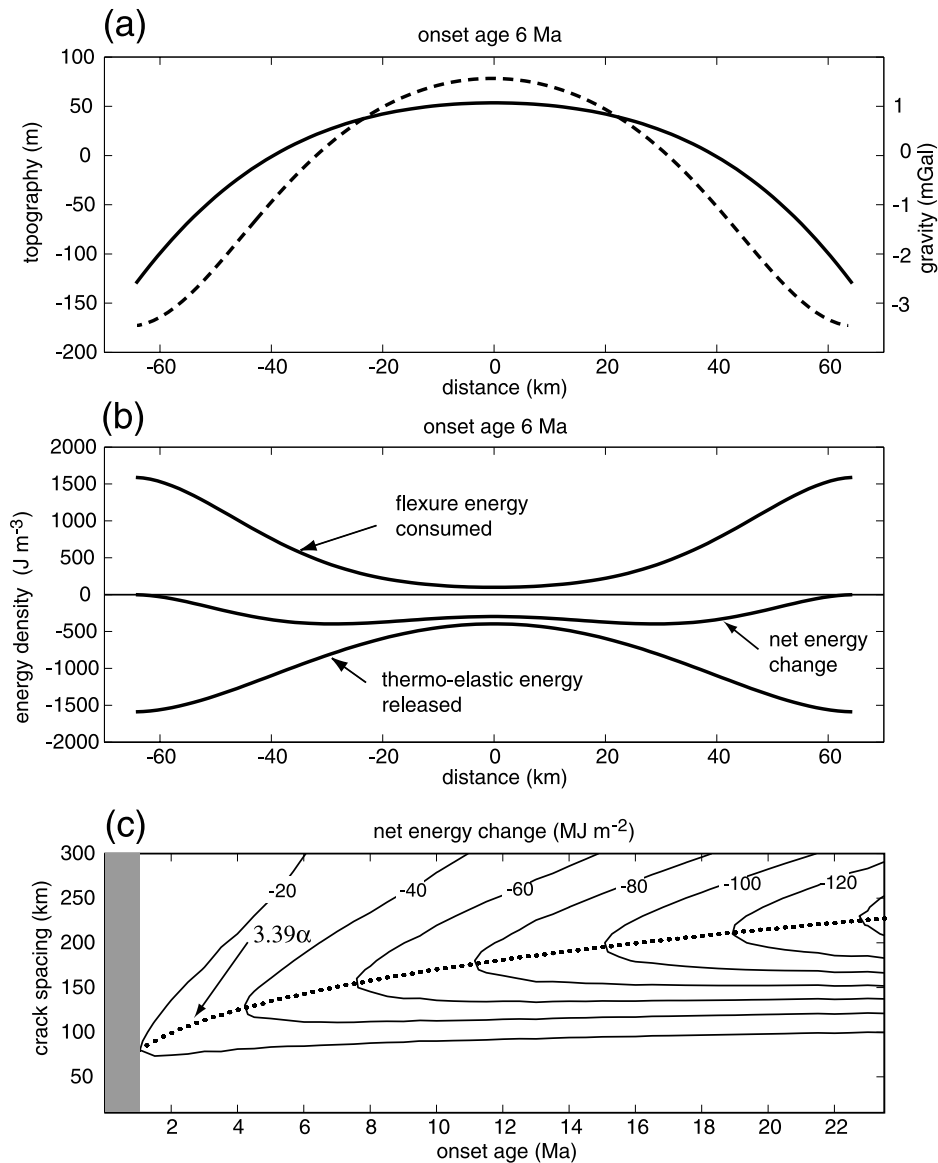


Figure 10. (a) Model of thermoelastic flexure where 130-km spaced cracks are introduced at 6 Ma (solid curve -230 m amplitude topography, dashed curve -5 mGal amplitude gravity anomaly). (b) Thermoelastic energy released by concave down bending exceeds energy consumed by flexing the plate. (c) Net energy versus crack spacing and crack onset age shows a minimum at 3.39 times the flexural parameter α .

the gravity lineaments near the ridge axis (Figure 1b) is interpreted as indicating a fracture resistance of the lithosphere to developing thermoelastic stress, our modeling results may be used to put an upper bound on the effective fracture energy of the lithosphere. For the parameters used in Figure 10, the corresponding energy is of the order of $QL/H \sim 10^7 - 10^8 \text{ Jm}^{-2}$.

[21] Our simple model explains both the wavelength and amplitude of the gravity lineaments observed on young seafloor (Figure 6). The solid curves in Figure 6 are the band-pass filtered gravity profiles at eight ages. The more regular gray curves are the predictions of the model using an onset age corresponding to the present seafloor age. These were computed by assuming uncompensated seafloor topography with uniform crustal thickness ($\rho_c =$

2800 kg m^{-3} ; $\rho_m = 3300 \text{ kg m}^{-3}$; 6 km crustal thickness). The model gravity profiles were low-pass filtered at 80-km wavelength to match the processing of the observed profiles and they were also scaled by 0.75 to provide a better match. This reduced amplitude may reflect incomplete cracking of the plate or an overestimate of Young's modulus used in the model calculation. The crack spacing is not perfectly regular so the model is unable to match the phase for more than about 2 undulations. We align a small section of the model profile to the data profile to illustrate the match in wavelength and amplitude. Note the agreement in amplitude and wavelength at ages of 0.5, 3.2, 5.7, and 8.2 Ma. At greater ages the model slightly overpredicts both the amplitude and the wavelength of the gravity anomalies. Of course, for the real oceanic lithosphere that ages continuously away from

the ridge axis, there is a third dimension that we have not considered. The gravity data alone are insufficient to answer the question of whether the lineaments developed suddenly in the past few million years in response to a plate-wide change in the stress field or whether the process has been continuous in time.

6. Conclusions

[22] Our improved gravity model derived from the ERS satellite altimeter data allows us to robustly resolve both the gravity lineaments and volcanic ridges on the central Pacific seafloor, as confirmed by comparisons with more limited shipboard surveys. We find that volcanic ridges preferentially occur in the troughs of the gravity lineaments. Modeling of the effects of the volcano-induced flexure on the gravity field demonstrates that the gravity lows cannot be explained by the volcanic loads, which essentially rules out a convective origin of the observed gravity lineaments. The satellite altimetry data indicate that lineaments are absent at the EPR axis but develop rapidly on young seafloor on both sides of the spreading ridge. On the Pacific plate they cross the grain of the older seafloor spreading fabric, suggesting that the gravity lineaments manifest an ongoing tectonic process. We develop a model for thermoelastic flexure of a cracked plate using well-constrained parameters of the plate cooling model and the yield strength envelope model. Elastic energy released by thermoelastic flexure has a pronounced maximum at a crack spacing of 3.4 times the flexural parameter of the cooling plate. Our model matches the wavelength and slightly over predicts the amplitude of the observed gravity lineaments. The thermoelastic cracking provides conduits for the escape of available magma to the surface resulting in volcanic ridge formation. The cracks are predicted to align perpendicular to the least compressive stress within the plate. The apparent obliqueness of the gravity lineaments to the older seafloor fabric implies a change in the stress orientation since the old fabric formation. This uniform orientation of the gravity lineaments combined with their increasing wavelength with increasing seafloor age, suggest they were initiated sometime during the past 5–7 Ma and their development continues today. Because the thermoelastic deformation is an intrinsic feature of the plate spreading, our model predicts that the seafloor corrugations and volcanic ridges should be ubiquitous features of the ocean basins. However, the more closely spaced transform faults on the slow spreading ridges (e.g., due to nonuniform magma supply to the ridge axis [Lin and Phipps Morgan, 1992; Fialko and Rubin, 1998]) may prevent the development of significant thermoelastic stress. Moreover, because the flexures have low amplitude (~200 m) they may only be observable on the flanks of the fastest spreading ridges where the sediment cover is minimal, and the ambient topography is smooth.

[23] **Acknowledgments.** We thank the Associate Editor Fredrik Simons and reviewers Doug Wilson and Ken MacDonald for their careful reviews and suggestions for improving the seamount analysis. We also thank David Naar for his critical comments. David Sandwell was supported by grants NSF OCE03-26707 and NASA NAG5-13673. Yuri Fialko was supported by grants OCE 0137226 and EAR 0208165. Correspondence and requests for materials should be addressed to David T. Sandwell (e-mail: dsandwell@ucsd.edu).

References

- Abers, G. A., B. Parsons, and J. K. Weisell (1988), Seamount abundances and distributions in the southeast Pacific, *Earth Planet. Sci. Lett.*, **87**, 137–151.
- Atkinson, B. K. (1987), *Fracture Mechanics of Rock*, pp. 1–23, Academic, San Diego, Calif.
- Bergman, E. A., and S. C. Solomon (1984), Source mechanisms of earthquakes near mid-ocean ridges from body waveform inversion, implications for the early evolution of oceanic lithosphere, *J. Geophys. Res.*, **89**, 11,415–11,444.
- Boley, B., and J. H. Weiner (1960), *Theory of Thermal Stress*, 586 pp., John Wiley, Hoboken, N. J.
- Bratt, S. R., E. A. Bergman, and S. C. Solomon (1985), Thermoelastic stress: How important as a cause of earthquakes in young lithosphere?, *J. Geophys. Res.*, **90**, 10,249–10,260.
- Buck, W. R., and E. M. Parmentier (1986), Convection beneath young oceanic lithosphere: Implications for thermal structure and gravity, *J. Geophys. Res.*, **91**, 1961–1974.
- Dunbar, J., and D. T. Sandwell (1988), A boudinage model for crossgrain lineations, *Eos Trans. AGU*, **69**, 1429.
- Fialko, Y. A. (2001), On origin of near-axis volcanism and faulting at fast spreading mid-ocean ridges, *Earth Planet. Sci. Lett.*, **190**, 31–39.
- Fialko, Y. A., and A. M. Rubin (1997), Numerical simulation of high pressure rock tensile fracture experiments: Evidence of an increase in fracture energy with pressure?, *J. Geophys. Res.*, **102**, 5231–5242.
- Fialko, Y. A., and A. M. Rubin (1998), Thermodynamics of lateral dike propagation: Implications for crustal accretion at slow-spreading mid-ocean ridges, *J. Geophys. Res.*, **103**, 2502–2514.
- Fleitout, L., C. Dalloubeix, and C. Moriceau (1989), Small-wavelength geoid and topography anomalies in the South Atlantic Ocean—A clue to new hot-spot tracks and lithospheric deformation, *Geophys. Res. Lett.*, **16**, 637–640.
- Forsyth, D., S. Webb, D. Scheirer, C. Langmuir, R. Duncan, and K. Donnelly (2002), COOK16MV Cruise Report R/V *Melville*: Tahiti-Easter I., 8 November–24 November, 2001, report, 20 pp., Brown Univ., Providence, R. I.
- Gans, K. D., D. S. Wilson, and K. C. Macdonald (2003), Pacific plate gravity lineaments: Diffuse extension or thermal contraction?, *Geochem. Geophys. Geosyst.*, **4**, 1074, doi:10.1029/2002GC000465.
- Goetze, C., and B. Evans (1979), Stress and temperature in the bending lithosphere as constrained by experimental rock mechanics, *Geophys. J. R. Astron. Soc.*, **59**, 463–478.
- Goodwillie, A. M., and B. Parsons (1992), Placing bounds on lithospheric deformation in the central Pacific Ocean, *Earth Planet. Sci. Lett.*, **111**, 123–139.
- Goodwillie, A. M., and A. B. Watts (1993), An altimetric and bathymetric study of elastic thickness in the central Pacific Ocean, *Earth Planet. Sci. Lett.*, **118**, 311–326.
- Haxby, W. F., and J. K. Weisell (1986), Evidence for small-scale mantle convection from Seasat altimeter data, *J. Geophys. Res.*, **91**, 3507–3520.
- Hussein, M. I. (1977), Energy balance for formation along a fault, *Geophys. J. R. Astron. Soc.*, **49**, 699–714.
- Janney, P. E., J. D. Macdougall, J. H. Natland, and M. A. Lynch (2000), Geochemical evidence from Pukapuka volcanic ridge system for a shallow enriched mantle domain beneath the South Pacific Superswell, *Earth Planet. Sci. Lett.*, **181**, 47–60.
- Lin, J., and J. Phipps Morgan (1992), The spreading rate dependence of three-dimensional mid-ocean ridge gravity structure, *Geophys. Res. Lett.*, **19**, 13–16.
- Lynch, M. A. (1999), Linear ridge groups: Evidence for tensional cracking in the Pacific plate, *J. Geophys. Res.*, **104**, 29,321–29,333.
- Maus, S., C. M. Green, and J. D. Fairhead (1998), Improved ocean-geoid resolution from retracked ERS-1 satellite altimeter waveforms, *Geophys. J. Int.*, **134**(N1), 243–253.
- Morgan, W. J. (1971), Convection plumes in the lower mantle, *Nature*, **230**, 42–43.
- Parmentier, E. M., and W. F. Haxby (1986), Thermal stress in the oceanic lithosphere: Evidence from geoid anomalies at fracture zones, *J. Geophys. Res.*, **91**, 7193–7204.
- Parsons, B., and J. G. Sclater (1977), An analysis of the variation of the ocean floor bathymetry and heat flow with age, *J. Geophys. Res.*, **82**, 803–827.
- Parsons, T., and G. A. Thompson (1991), The role of magma overpressure in suppressing earthquakes and topography: Worldwide examples, *Science*, **253**, 1300–1302.
- Ricard, Y., and C. Froidevaux (1986), Stretching instabilities and lithospheric boudinage, *J. Geophys. Res.*, **91**, 8314–8324.
- Richter, F. M., and B. Parsons (1975), On the interaction of two scales of convection in the mantle, *J. Geophys. Res.*, **80**, 2529–2541.

- Sandwell, D. T. (1986), Thermal stress and the spacings of transform faults, *J. Geophys. Res.*, *91*, 6405–6417.
- Sandwell, D. T., and W. H. F. Smith (1997), Marine gravity anomaly from Geosat and ERS-1 satellite altimetry, *J. Geophys. Res.*, *102*, 10,039–10,054.
- Sandwell, D. T., E. L. Winterer, J. Mammerickx, R. A. Duncan, M. A. Lynch, D. A. Levitt, and C. L. Johnson (1995), Evidence for diffuse extension of the Pacific plate from Pukapuka ridges and cross-grain gravity lineations, *J. Geophys. Res.*, *100*, 15,087–15,099.
- Scholz, C. H. (2002), *The Mechanics of Earthquakes and Faulting*, 496 pp., Cambridge Univ. Press, New York.
- Searle, R. C., J. Francheteau, and B. Cornaglia (1995), New Observations on mid-plate volcanism and the tectonic history of the Pacific plate, Tahiti to Easter Microplate, *Earth. Planet. Sci. Lett.*, *131*, 395–421.
- Shen, Y., D. W. Forsyth, J. Conder, and L. M. Dorman (1997), Investigation of microearthquake activity following an intraplate teleseismic swarm on the flank of the Southern East Pacific Rise, *J. Geophys. Res.*, *102*, 459–475.
- Sleep, N. H. (1992), Hotspot volcanism and mantle plumes, *Annu. Rev. Earth Planet. Sci.*, *20*, 19–43.
- Smith, W. H. F., and D. Sandwell (1997), Global seafloor topography from satellite altimetry and ship depth soundings, *Science*, *277*, 1956–1962.
- Turcotte, D. L. (1974), Are transform faults thermal contraction cracks?, *J. Geophys. Res.*, *79*, 2573–2577.
- Wessel, P. (1992), Thermal stress and the bimodal distribution of elastic thickness estimates of the oceanic lithosphere, *J. Geophys. Res.*, *97*, 14,177–14,193.
- Wessel, P., and W. H. F. Smith (1991), Free software helps map and display data, *Eos Trans. AGU*, *72*, 441, 445–446.
- Wiens, D. A., and S. Stein (1984), Intraplate seismicity and stress in young oceanic lithosphere, *J. Geophys. Res.*, *89*, 11,442–11,464.
- Winterer, E. L., and D. T. Sandwell (1987), Evidence from en-echelon cross-grain ridges for tensional cracks in the Pacific plate, *Nature*, *329*(6139), 534–537.
- Woo, T. C. (1968), Thermal stress problems in glass, *J. Appl. Phys.*, *39*(4), 2082–2087.
-
- Y. Fialko and D. Sandwell, Scripps Institution of Oceanography, University of California, San Diego, IGPP 0225, La Jolla, CA 92093-0225, USA. (dsandwell@ucsd.edu)